Design and Numerical Simulation of a Micro-Gas Turbine Combustor

P. Zhang, Y. P. Liu, J. H. Li and Y. W. Yan[†]

Aero-engine Thermal Environment and Structure Key Laboratory of Ministry of Industry and Information Technology, Nanjing University of Aeronautics and Astronautics, Nanjing 210016, China

†*Corresponding Author Email: yanyw@nuaa.edu.cn*

ABSTRACT

A cannular combustor with a 100-KW thermal power was designed with a swirler, primary holes, dilution holes, and cooling holes based on an original gas turbine of a practical application. Further, the combustion process in this combustor was numerically simulated by using Computational Fluid Dynamics (CFD). A methane-reduced chemical mechanism was applied to CFD to simulate the combustion process. The combustion performance, product concentrations, and flow field were analyzed. Experimental data of airflow distribution obtained in previous study were applied in the design process. The present work was reported to verify that the experimental data can be regarded as a guide and optimization basis in the aerodynamic design process. Additionally, the consistency of numerical results and design data indicates that the design in this paper could satisfy the design requirements.

Keywords: Cannular combustor; Numerical simulation; Turbulent combustion; Combustion mechanism.

1. INTRODUCTION

The micro gas turbine is a developing type of thermal engine, which is extensively used in ground generators. The design process of a combustor is slightly different from that of an aircraft owing to the usage of different types of fuel. The kerosene is used in aircraft while natural gas in ground generators. Considerable experience and experimental data are applied during the design process. The airflow distribution should be initially considered to obtain a reliable flow field. Further, the combustion performance can be observed by conducting a numerical simulation.

Several experimental and numerical studies have been conducted on micro-gas turbine combustors, both domestically and abroad. Various types of micro-gas turbine combustors have been proposed (Zhang and Feng, 2003; Zhang and Feng, 2005; Yang, 2016), and the differences between the characters of actual thermal flow field and the design index, such as total pressure recovery coefficients, the exit temperature, mass flow rate, and et, have been investigated (Zhang and Feng, 2005). Furthermore, the influence of the flow control plate on the temperature field at the exit and the distribution of pollutants have been discussed (Zhang and Feng, 2005). The detailed flow analysis has been conducted to discover the basic law between velocity and temperature profiles by considering the link among the internal flow field and exit parameters and the total quantity of air supplied (Yang, 2016). Using the "Fortran" and Delphi codes, a combustor design program has been developed to not only simplify the design process but also to predict the aerodynamic parameters and the liner wall temperature (Lin, 2013). Further, the influence of vane angle on the outlet temperature pattern factor was analyzed. By appropriately decreasing the angle, the exit temperature distribution can be improved (Liu *et al*. 2017). Gordon *et al*. (2005) described a detailed simulation of the YT-175 engine combustor. The entire flow field was modeled, ranging from the compressor diffuser to the turbine inlet. Further, the temperatures of the vaporizer and the liner walls were predicted and compared with the measured test data. An agreement could be observed between the calculated and measured values. In the TECFLAM combustor, a presumed PDF model with respect to temperature fluctuations was employed to numerically simulate the turbulent swirling flame of methane. The calculated axial, radial, and tangential velocities of the gas and mass fractions, temperature, and temperature fluctuation of species agreed well with the experimental data

(Yang, 2009). An oxygen–methane diffusion flame in a gas turbine combustor was experimentally investigated under various operating conditions. The flame stabilization mechanism was investigated, and it was observed that both the flame and fuel-gas temperatures decreased with an increasing equivalence ratio (Habib *et al*. 2015). In terms of large eddy simulations, a methane-reacting flow was simulated in an industrial gas turbine combustor that was operated at a pressure of 3bar. A reduced GRI 3.0 mechanism containing 15 reaction steps and 19 species was introduced. The results at different axial locations were observed to be similar with the measured data, which verified that the CFD methods can be used to solve complicated turbulent combustion problems (Bulat *et al*. 2011).

With different combustion chamber shapes, combustion performance of a diesel engine, was numerically investigated, especially the speed, temperature, discharge and gas flow (Cao and Li, 2018).Under various swirl numbers, the flow field, temperature field and thermal NOₓ formation rate in the combustor were analyzed on a heavy gas turbine. With swirl number increase, the recirculation zone enlarged and the temperature peak decreased, then the thermal NOₓ formation decreased (Ge and Fu, 2018). A new concept of reverse fuel injection was proposed (Rajpara *et al*. 2018). It declared to enhance the fuel-burning rate in upward swirl cannular combustor. Experiments and simulations indicated that reverse fuel injection could improve combustion efficiency and reduction in CO emission. And the injection length could influence the total pressure loss a lot. Saboohi *et al*. (2018) focused on the conceptual design of a conventional gas turbine combustor by the multi-objective optimization method. It aimed to optimize the emission indices, airflow distribution, and the length of combustion zone. Results suggested that minor changes could mattes much to obtain an acceptable solution.

As one of the three major components, the combustor plays an important role in a gas turbine. Further, the combustor can directly affect the lifespan and power output of a turbine. In this study, a combustor modeling process and combustor structures are initially introduced. A CFD software application called Fluent is used to simulate the flow field inside the liner to obtain the flow structure and various performance indexes, which are subsequently used to derive an optimal model that is applied for detailed combustor simulation.

2. DESIGN PROCESS

The combustor is considered to be the major component in a gas turbine. In the combustor, the chemical energy is converted to thermal energy via the combustion of an air–fuel mixture.

Hot gases are produced after the fuel–oxygen reaction, and these gases are subsequently cooled by the fresh air admitted from dilution holes to achieve a suitable exit temperature profile for protecting the turbine blades from ablation. While the turbine blades are operated in a high-temperature environment for extended durations, a certain amount of ablation is observed to occur, and the blade life and reliability exhibit a considerable decrease.

2.1 Conceptual Design

In present work, a cannular combustor was designed, with a given operating condition, which must satisfy a range of basic requirements. According to a practical application, the design criteria concerned in this paper are listed as follows:

1. High-combustion efficiency (>99%).

2. Low pressure loss. The total pressure loss coefficient is limited to 4%.

3. A suitable exit temperature distribution, which varies due to different pattern factor, at least satisfies normal range.

4. Reliable ignition and stable combustion performance at a given operating condition.

More detailed design criteria, such as low emission, durability, will be proposed in further investigations. The design conditions were showed in Table 1.

Table 1 Known conditions for design process

Operating conditions	---
Inlet airflow mass rate	0.9kg/s
Inlet airflow temperature	473K
Inlet airflow pressure	400bar
Outlet gas temperature	1200K
Inlet fuel pressure	640bar
Calorific value of fuel	39MJ/Nm³

In the conceptual phase, several simple empirical formulas are applied to determine the outline of the combustor while preparing the detailed design process. The conceptual design process (Xin and Zhong, 2015) is depicted in Fig. 1.
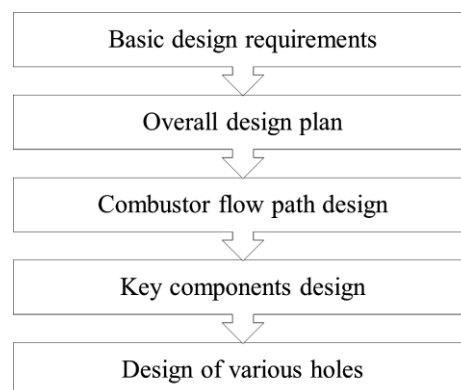

Fig. 1. Conceptual design process.

2.2 Experiments on Airflow Distribution

The air flow distribution in the combustor considerably influences the combustion

performance. According to the project requirements, it is expected that the airflow distribution does not change too much with the different combustor inlet conditions (He *et al.* 2018).

Owing to the limitations of turbines, and liner materials, and cooling technologies, the total fuel-air ratio in a combustor is lower than the stoichiometric ratio. Therefore, flame stability in the primary, dilution, and downstream cooling zone, as well as the exit temperature, must be considered. (Lin, Xu and Liu, 2008)

Because of the limitations of turbines, liner materials, and cooling technologies, the total fuel–air ratio in a combustor is observed to be lower than the stoichiometric ratio. Therefore, flame stability in the primary, dilution, and downstream cooling zone along with the exit temperature must be considered (Lin, Xu and Quan, 2008).

During previous investigations, experiments pertaining to airflow distribution have been conducted (He *et al*. 2018). A cannular combustor with a 100-KW thermal power, which is the original model for the design process, was used to perform these experiments. The experimental data that were obtained in these investigations could serve as a reference to achieve a suitable combustor design and optimization in the present study.

The experimental system used in this study is presented in Fig. 2. Air was supplied to the combustor using a screw air compressor, and the mass flow rate of air was adjusted using the vent valve of the compressor. Further, the air flow through the inlet duct and the mass flow rate were measured using a vortex flow meter that was installed in the measurement section upstream of the combustor. The experiment was performed under the atmospheric pressure condition, and the total pressure of each component was observed to be considerably smaller than the atmospheric pressure. Therefore, the drainage method, in which the change of pressure was converted to the rise of the water level in pressure measuring pipe, was adopted for measuring pressure so as to obtain accurate pressure values. The total pressures of the inlet and outlet in the combustor were measured at the demarcated measuring points in the inlet and outlet ducts. Further, an L-shaped total pressure measuring pipe was employed to ensure that the pipe was exactly opposite to the airflow. The hole-plugging method was used to obtain the airflow distribution characteristics of the swirler, primary holes, and dilution holes. After completing the measurement, the air was expelled to the atmosphere.

Initially, in Fig. 3, the airflow distribution characteristics of the swirler, primary holes, and dilution holes were experimentally observed under atmospheric pressure to obtain accurate pressure measurements.

Further, the pressure differentials of the swirler, primary holes, and dilution holes were measured under different airflow inlet conditions. According

to the airflow distribution characteristics, the actual air mass flow can be obtained under a given inlet condition. The experimental data is summarized in Table 2.
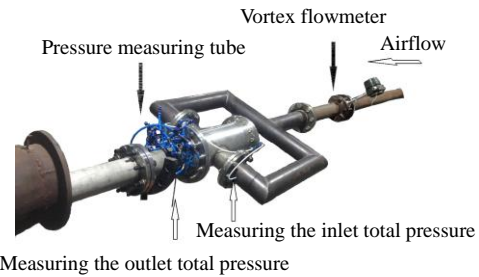

Fig. 2. Experimental system.
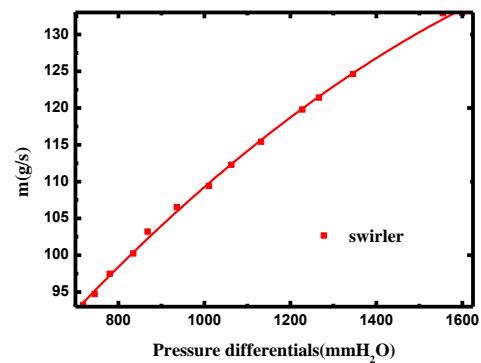
(a) The flow characteristics of swirler
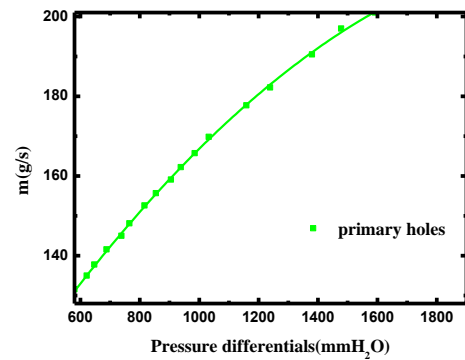
(b) The flow characteristics of primary holes
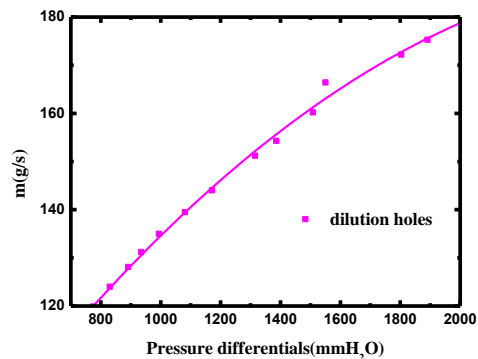
(c) The flow characteristics of dilution holes
Fig. 3. Airflow distribution characteristics.

Table 2 Experimental data obtained

W(g/s)	W_s	W_{ph}	W_{dh}	W_c
283.82	21.61%	33.21%	26.89%	18.29%
409.11	22.10%	33.49%	26.91%	17.50%
450.92	22.11%	33.46%	27.21%	17.21%
468.60	22.66%	33.63%	27.57%	16.13%
491.02	22.65%	33.75%	27.64%	15.97%
510.85	22.63%	33.94%	27.60%	15.83%
539.73	22.62%	33.72%	27.53%	16.12%

W represents total airflow rate; W_* denotes the airflow distribution coefficient. W_s: swirler airflow; W_{ph}: primary air jet; W_{dh}: dilution air jet; W_c: total cooling air In addition, the inlet and outlet total pressure in the combustor were obtained with the swirler, primary holes, dilution holes, and cooling holes all remaining open. Then the total pressure loss coefficient can be calculated, as shown in Table 3.

Table 3 Experimental data obtained

Mass Flow Rate (g/s)	Inlet Reynolds Number	Pressure loss coefficient
283.8	196918	4.42%
409.1	283790	5.94%
428.5	297320	6.53%
450.9	312863	7.26%
468.6	325144	8.08%
491.0	340687	8.78%
510.8	354425	9.54%
539.7	374478	10.67%

Since experimental pressure loss is concerned with the inlet air flow of the combustor, the design conditions need to be converted to the experimental operations according to the equal Mach number principle in the inlet. The experiment was carried out under atmospheric pressure and normal temperature, 20 degrees. Actual inlet operation can be calculated as follow:

$$\mathrm{M}_a = \frac{u}{c} = \frac{m}{\rho A}\frac{1}{c} \Rightarrow m_1 = 0.9 kg/s, m_2 = 0.286 kg/s \qquad (1)$$

As the inlet mass flow rate equals to 285g/s, it is exactly corresponding to the design point, and at that time, the pressure loss coefficient is 4.42%.

Moreover, the desired airflow distribution in an aerodynamic design can be obtained as follows: atomization airflow = 22%, primary jet = 33%, dilution jet = 27% and cooling airflow = 17%. In the present study, the experimental data were initially regarded as a predicted airflow distribution in the combustor flow path design process and as a reference for further optimization of the airflow distribution design.

3. COMBUSTOR STRUCTURE

In the present study, a combustor was designed for micro generators, which are required for ensuring operation in an economic and reliable manner over long periods without attention (Lefebvre and Ballal,

2010). Several key parts, including the swirler, primary holes, dilution holes, and cooling holes, have supported reasonable combustion, cooling effect, wall temperature, and outlet temperature profile. Under condition of strong swirl, the fuel is rapidly mixed with the swirling air in the combustor, in which the combustion is close to semi-premixed. A large number of small cooling holes were created to reduce the wall temperature to protect the liner part and to prolong the service life of the generator. The main configurations of this combustor are presented in Fig. 4.

3.1 Fuel-Air Ratio

Assuming that the gases at inlet and outlet were regarded as incompressible, perfect gases, according to energy conservation equation, the total fuel-air ratio was calculated to be 0.017, to provide a lean combustion. While at the primary zone, the fuel-air ratio was designed to be 0.058, and the mixed flow was exactly stoichiometric.

3.2 Combustor Flow Path Design

Combustor flow path design was generally based on previous design experiences (Xin and Zhong, 2015; Lefebvre and Ballal, 2010; Meller, 1990; Jin and Suo, 2016). With the velocity method, dome preference velocity was selected to be 5.6m/s, then combustor maximum area (A_{ref}) could be calculated from continuity.

On basis of design experiences, the design parameters were selected as follows:

Diameter of flame tube:

$$D_{ref} = \sqrt{4A_{ref}/p} = 131\text{mm} \qquad (2)$$

Combustor length:

$$L = (2.5 \sim 3.5) D_{ref} = 405\text{mm} \qquad (3)$$

Combustion zone length:

$$L_c = (1.8 \sim 2.0) D_{ref} = 270\text{mm} \qquad (4)$$

Primary and Dilution zone length:

$$L_{ph} = L_{dh} = (0.9 \sim 1.5) D_{ref} = 135mm \qquad (5)$$

Transition tube:

$$L_m = L - L_c \qquad (6)$$

The combustor was divided into the primary zone, dilution zone, and a transition part, the total length was 405mm. The maximum diameter and total length of the outer casing were 180 and 450 mm, respectively.

3.3 Swirler and Injector

Swirler design did matter much to flame stabilization. A flame can be stabilized on account of the recirculation of high-temperature gas and air–fuel. The main objective of a swirler is to create a recirculation zone based on the principle of vortex entrainment by which a low-pressure core is formed. Because of the continuous flow of hot gas

upstream, a self-compensating ignition source is formed, which is necessary to maintain the flame stability. Further, the swirl vane angle can be adjusted to investigate the influence of various angles on the exit temperature profile and combustion performance.

In this work, an axial swirler was selected. Main design variables were:

Vane angle: $50°$

Vane thickness: 1mm

Number of vanes: 12

Outer diameter:

$$D_o = (0.35 \sim 0.50) D_{ref} = 46mm \qquad (7)$$

Inner diameter: $D_i = (0.45 \sim 0.75) D_o = 23mm \qquad (8)$

Injector length: $L_i = 45mm \qquad (9)$

A plain orifice injector was employed in this combustor. The methane, under high pressure from a gas pipe, would be injected to hot airflow from several inclined holes. The combination of swirler and injector was showed in Fig. 4.
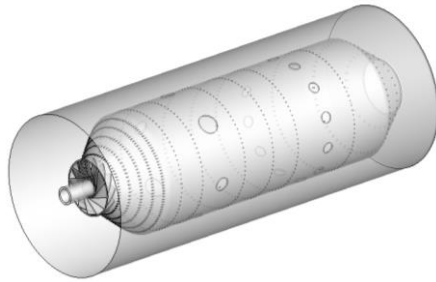
Fig. 4. Combustor model.

3.4 Holes Structure

With a desired airflow distribution, the flow area of each component could be determined from continuity. Thus, it can be seen in Fig. 4, that the liner surface contained six primary holes and ten dilution holes, and they were uniformly distributed along the circumferential direction.

In the dome, fuel was abundant to provide a rich ignition; and, a part of fresh air flowing through the primary holes was introduced upstream and supplied for combustion.

Furthermore, the primary airflow acted to cut off the recirculation zone for avoiding the expansion of the hot gas toward the exit. The six primary holes - $\Phi22mm \times 2, \Phi15.6mm \times 4$ -were located in the distance of 135mm from the injector exit.

Another flow was the feed across the dilution holes, which was employed to eliminate heat from the hot gas and to achieve a suitable exit temperature distribution. Ten dilution holes- $\Phi18mm \times 4$ -were located in the distance of 270mm from the injector exit.

The stream of cooling air made an angle of 35° with the main stream. Total cooling area was 0.0004464m². A cooling film grew near the liner wall, and this film served to extend the life of the liner part over a range of operating temperatures. All the main components are depicted in Fig. 4.

4. SIMULATION AND OPTIMIZATION

4.1 Math Model and Simulation Methods

Four basic governing equations should be considered for investigating the turbulent combustion in a gas turbine combustor, including continuous equations, momentum conservation equations, energy conservation equations, and species equations. These equations were given:

Continuous equations:

$$\frac{\partial \rho}{\partial t} + \frac{\partial (\rho u)}{\partial x} + \frac{\partial (\rho v)}{\partial y} + \frac{\partial (\rho w)}{\partial z} = 0 \qquad (10)$$

ρ means density of fluid; t means time; And u, v, w denotes the vector velocity in three directions x, y, z.

Momentum conservation equations:

$$\frac{\partial (\rho u)}{\partial t} + \frac{\partial (\rho uu)}{\partial x} + \frac{\partial (\rho uv)}{\partial y} + \frac{\partial (\rho uw)}{\partial z}$$
$$= \frac{\partial \left(\mu \frac{\partial u}{\partial x} \right)}{\partial x} + \frac{\partial \left(\mu \frac{\partial u}{\partial y} \right)}{\partial y} + \frac{\partial \left(\mu \frac{\partial u}{\partial z} \right)}{\partial z} - \frac{\partial p}{\partial x} + S_u \qquad (11)$$

$$\frac{\partial (\rho v)}{\partial t} + \frac{\partial (\rho vu)}{\partial x} + \frac{\partial (\rho vv)}{\partial y} + \frac{\partial (\rho vw)}{\partial z}$$
$$= \frac{\partial \left(\mu \frac{\partial v}{\partial x} \right)}{\partial x} + \frac{\partial \left(\mu \frac{\partial v}{\partial y} \right)}{\partial y} + \frac{\partial \left(\mu \frac{\partial v}{\partial z} \right)}{\partial z} - \frac{\partial p}{\partial y} + S_v \qquad (12)$$

$$\frac{\partial (\rho w)}{\partial t} + \frac{\partial (\rho wu)}{\partial x} + \frac{\partial (\rho wv)}{\partial y} + \frac{\partial (\rho ww)}{\partial z}$$
$$= \frac{\partial \left(\mu \frac{\partial w}{\partial x} \right)}{\partial x} + \frac{\partial \left(\mu \frac{\partial w}{\partial y} \right)}{\partial y} + \frac{\partial \left(\mu \frac{\partial w}{\partial z} \right)}{\partial z} - \frac{\partial p}{\partial z} + S_w \qquad (13)$$

In these equations, p and μ respectively represent the pressure in the surface of fluid cell and viscosity of fluid; S_u, S_v, and S_w were volume force in three directions.

Energy conservation equations:

$$\frac{\partial (\rho T)}{\partial t} + \frac{\partial (\rho uT)}{\partial x} + \frac{\partial (\rho vT)}{\partial y} + \frac{\partial (\rho wT)}{\partial z}$$
$$= \frac{\partial \left(\frac{\lambda}{C_p} \frac{\partial T}{\partial x} \right)}{\partial x} + \frac{\partial \left(\frac{\lambda}{C_p} \frac{\partial T}{\partial y} \right)}{\partial y} + \frac{\partial \left(\frac{\lambda}{C_p} \frac{\partial T}{\partial z} \right)}{\partial z} + S_T \qquad (14)$$

Where T means temperature of fluid; λ, C_p, and S_T

were the thermal conductivity, specific heat capacity and viscous dissipation.

Species equations:

$$\frac{\partial(\rho Y_s)}{\partial t}+\frac{\partial(\rho u Y_s)}{\partial x}+\frac{\partial(\rho v Y_s)}{\partial y}+\frac{\partial(\rho w Y_s)}{\partial z} \qquad (15)$$

$$=\frac{\partial\left(\rho D_s \frac{\partial Y_s}{\partial x}\right)}{\partial x}+\frac{\partial\left(\rho D_s \frac{\partial Y_s}{\partial y}\right)}{\partial y}+\frac{\partial\left(\rho D_s \frac{\partial Y_s}{\partial z}\right)}{\partial z}-w_s$$

Where Y_s and D_s mean the mass fraction and diffusion coefficient of specie s, and w_s represents the production or consumption of specie s owing to chemical reactions inside the cells.

According to the Reynolds-average method, the Standard k-epsilon turbulent model (Jones and Launder, 1972) was adopted in simulations for enclosing the Reynolds stress. The finite volume method was used to discretize the fields in the CFD software that can be referred to as Fluent. The difference equations using the finite volume method were accurately solved using SIMPLE, which is a semi-implicit algorithm-based staggered-grid method.

Further, the real chemical reaction in turbulent combustion is so complex that it is difficult to analyze the concentration and distribution of various complex components in detail. In a rough simulation of the internal fields in combustor, it is imperative to consider the combustion performance.

Therefore, to simulate the global reaction combustion instead of considering complex chains reactions, the "simple chemical reaction system" model (Spalding, 1980) has been assumed and the eddy dissipation model (EDM) (Magnussen and Hjertager, 1976) was selected in the present work.

With the introduction of methane reduced mechanism, the eddy dissipation concept (EDC) model (Magnussen, 1981) was used to simulate complex chemical reaction mechanisms in Fluent.

The eddy-dissipation model, a turbulence-chemistry interaction model, was provided in Fluent. With this model, for any species i, the net rate of production was given by the smaller of these two expressions below:

$$R_{i,\mathrm{r}}=v_{i,r}^{'} M_{w,\mathrm{i}} A\rho\frac{\varepsilon}{k}\min_R\left(\frac{Y_R}{v_{R,\mathrm{r}}^{'} M_{w,R}}\right) \qquad (16)$$

$$R_{i,\mathrm{r}}=v_{i,r}^{'} M_{w,\mathrm{i}} AB\rho\frac{\varepsilon}{k}\frac{\sum\limits_P Y_P}{\sum\limits_j^N v_{j,r}^{"} M_{w,j}} \qquad (17)$$

Where Y_P means the mass fraction of any product species P; while Y_R is the mass fraction of a certain reactant R; k,ε are kinetic energy and dissipation rate; and A, B equal to 4.0, 0.5; these subscripts such as i, j, P, R, declare different species.

The eddy dissipation concept model was extended based on the eddy-dissipation model. Detailed chemical mechanism was allowed in turbulent flow. And a new term-the fine scales was introduced to modify the source term in the conservation equation.

4.2   Modeling and Mesh Description

For grid meshing, grids of different sizes were selected considering the complexity of the combustor geometry, and an unstructured grid was generated using Gambit. A local mesh refinement was applied to a thin layer adhered to the inner linear part and small holes. A mesh model with 6425621 cells was selected after verification of grid independence. The mesh map is shown in Fig. 5.

4.3   Boundary Conditions

The boundary conditions that are involved in the simulation are as follows:

(1) Inlet conditions: The model combustor contained gas and air inlets. For a given mass flow rate, the airflow mass rate was 0.9 kg/s, while the gas flow mass rate was 0.0153 kg/s. Further, the temperature and pressure were determined by a fixed value. The velocity vector was specified to be normal to the boundary. The two key parameters of turbulence combustion are intensity and hydraulic diameter of the tube, and both the parameters can be predicted.

In this study, the flow path exhibited almost a round tubular path. Therefore, the hydraulic diameter was exactly the same as the inner diameter of the tube. The oxygen concentration of the air inlet was set to 0.23, while the methane concentration was set to 1 at the gas inlet.

(2) Outlet conditions: The velocity and pressure at the exit were unknown. Hence, the outflow boundary condition was selected.

(3) Wall conditions: The default standard wall function in Fluent was accepted. And, the specific wall temperature is not a considered objective. Only the fluid region will be used in the simulation, and the fluid-solid coupling is not involved, so the radiation and heat transfer coefficients could be ignored. Further studies about wall temperature would be carried out.

In terms of the operating conditions, the reference pressure was set to 400bar and was located within the fluid domain.

4.4   Results and Analysis

In this section, four slices are extracted for detailed analysis: Face A: longitudinal section at the combustor center, and located in x=0; Face B: a slice crossing through the center of all primary holes and normal to Face A, and located in z=135mm; Face C: a slice crossing through the center of all dilution holes and normal to Face A, and located in z=270mm; Face D: combustor exit. The locations of the sampling faces are depicted in Fig. 6.

4.4.1 Non-Reacting flow

The influence of the chemistry reaction on the internal flow field in the combustor can be considered to be negligible in case of a non-reacting flow, and the only matter that must be focused on is the process of gas–air mixing and co-circulation. A cold flow field is considerably significant from the viewpoint of the combustion flow structure. A reasonably cold flow field helps with the subsequent investigations.


Fig. 5. Mesh description.

Plane：x=0   Plane：z=135mm
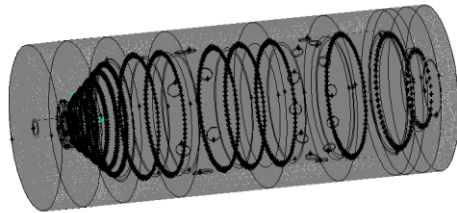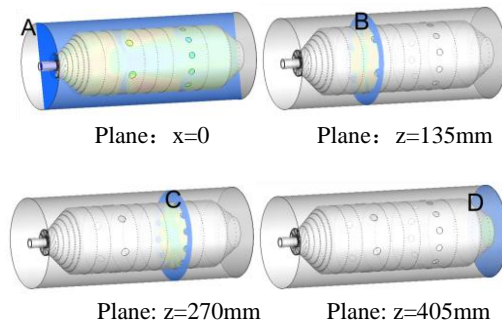
Plane: z=270mm   Plane: z=405mm
Fig. 6. Slice locations.

The velocity vector and isogram contour are depicted in Fig. 7. and Fig. 8. The simulation results exhibit that the recirculation zone was symmetrically distributed inside the combustor. The airflow crossing through the axial swirl turned into swirling jets, and a low-pressure zone was rapidly formed under this condition; a recirculation zone was formed in this low-pressure zone. Furthermore, the additional airflow admitted from the primary holes may have been drawn upstream owing to the presence of a low-pressure core. Additionally, almost half of the additional airflow flowed back to the primary zone in addition to the vortex produced in the recirculation zones, both of which can accelerate the reaction rate and the heat release rate. The recirculation zones made it possible to stabilize a continuous ignition source at a certain location, which is an important precondition for performing the flame-holding measurements. A cooling film flowed along the liner surface, which proved the effectiveness of the cooling technique. The entire flow field was symmetrical and similar to the true flows in actual projects.

Generally, the recirculation and dilution processes are advantageous when the jet depth is 0.5–0.7 times that of the combustor half-height (Jiao, 1981). It can be concluded that in Fig. 8, the jet depth of

both the primary and the dilution holes is almost uniform around the tube. The primary jet height is as deep as 0.7 times the combustor half-height. The air jet was fed into the combustion zone to rapidly combine and react with the unburned gas; this further increased the combustion efficiency. Meanwhile, the dilution jet was approximately 0.5–0.6 times the combustor half-height, and the cold airflow could cool the hot gas to a reasonable exit temperature pattern factor by diluting it with the burned mixture.
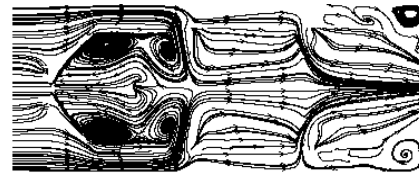

**Fig. 7. Velocity streamline of non-reacting flow.**

A:
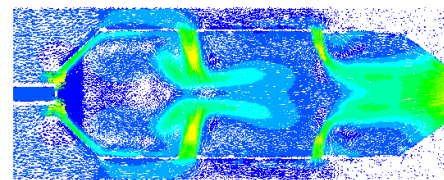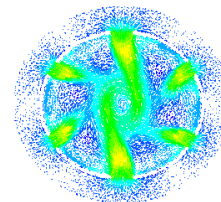
B: C:
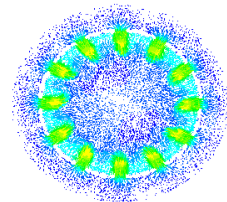
Fig. 8 Velocity vector contour of non-reacting flow.

4.4.2 One-Step Reacting flow

The combustion state is the major object that has to be monitored during the reacting flow simulation. The temperature field in various sections is depicted in Fig.9.

The two peaks of the flame are clear and are symmetrically located on surface A. The flame structure and location in the combustor are reasonable, and a high-temperature zone is formed behind the primary holes. The fresh air was combined with a small amount of unburned mixture in the downstream region, and a further reaction occurred that released the additional heat to warm the mixture. Meanwhile, the cooling film near the liner surface worked in an effective manner to shield the liner part from heat. Additionally, the primary jets were effective for reducing the primary recirculation zone. A suitable secondary airflow can effectively strengthen the combustion. Therefore, the exposed surface area gradually increased with

increasing amounts of inflow of fresh air, which accelerated the reaction rate. Combined with the temperature contour on the C-plane, the secondary airflow was successful in reducing the temperature of the hot gas flowing in from the combustion region. The average outlet temperature was approximately 1200 K, and the exit temperature distribution is depicted in Fig.10. The combustion efficiency was calculated to be 99.6% from the temperature method (Aero-engine Design Manual, 2001). Thus, the temperature field was observed to be relatively reasonable.

A:

B: C:
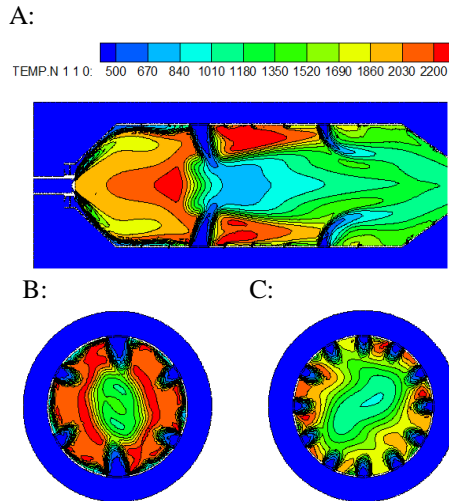
Fig. 9. Temperature contour of reacting flow (TEMP: temperature/K).

The temperatures at different locations along the axial direction of the combustor are plotted in Fig.11. High-pressure methane was injected from an injector with an initial temperature of 300 K. It was instantly mixed with the swirling air. Further, the mixture reaction occurred. The center of the nozzle exit was located at z = 0 mm. Notably, the temperature along the axial direction increased to almost 1800 K when the methane was stretched out. At z = 0–45 mm, where the dome existed, the temperature continued to increase along the central axis. In the recirculation zone, the fresh mixture was preheated by the hot gas in the upstream region, and large quantities of active carriers were produced, which promoted the chemical reaction rate. Furthermore, cooling jets were injected through the primary holes, and they were subsequently injected into the hot unburned gas, which accelerated the reaction and released large amounts of heat, resulting in elevated temperatures. In the meantime, the hot gas region was separated by a vast airflow from the primary holes; subsequently, the temperature along the central axis was relatively low. Owing to the long distance from the injector exit, the surrounding hot gas started spreading in the central region in which the temperature was observed to be relatively increased. After the hot gas was completely mixed with the cold air entering through those holes, the temperature tended to remain constant; hence, a suitable exit temperature was achieved.
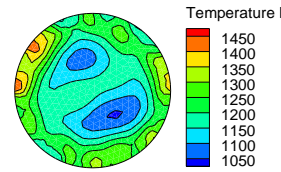

**Fig. 10 Exit temperature distribution.**
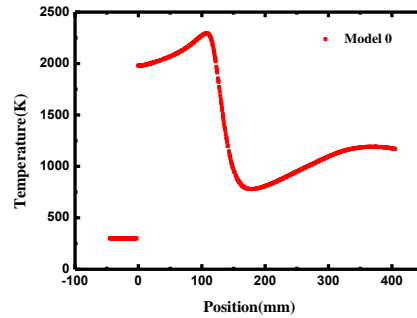
Fig. 11 Temperature at different axial locations.

The total pressure loss coefficient in the numerical simulation of one-step reacting flow was approximately 3.09%, which was calculated as follows:

$$\varepsilon = \frac{p_3^* - p_4^*}{p_3^*} \quad (18)$$

In this equation, p_3^* is the inlet total pressure, and p_4^* is the outlet total pressure.

The pattern factor referred to as overall temperature distribution factor (OTDF) is commonly used for evaluating the outlet temperature distribution, which is tailored to maximize the lives of turbine blades and nozzle guide vanes. Typically, OTDF should vary from 0.25 to 0.35 (Huang and Lin, 2001); otherwise, the turbine blades may be damaged. The factor can be defined as follows:

$$OTDF = \frac{T_{max} - T_{4ave}}{T_{4ave} - T_{3ave}} \quad (19)$$

T_{4max} is the maximum of the exit temperature; T_{4ave} is the average temperature at the exit; $T_{4ave} - T_{3ave}$ is the average increase in temperature.

The maximum and minimum exit temperatures in the simulation were 1440.68 K and 1049.89 K, respectively. The initial and final mixture temperatures were 417 K and 1197.71 K. Further, the pattern factor was calculated to be 0.33, which was acceptable.

Above all, the simulation results were collected to compare with the design point, in Table 4. It suggested that most of the numerical data would satisfy the design requirements.

While the swirl airflow was insufficient，which resulted in imperfect combustion. The airflow distribution is needed to be further optimized.

Table 4 Comparison between design and numerical data

	Design Data	Numerical Data
Combustion efficiency	99%	99.6%
Airflow distribution	22%,37%, 27%,17%	15.5%,32.4%, 37.4%,14.7%
Total pressure loss coefficient	4%	3.1%
Mean exit temperature	1203K	1200K
Exit temperature factor	0.25~0.35	0.31

4.4.3 Optimization

Five optimizations were proposed based on the initial result obtained from the simulation performed using model 0. Based on the analyses, the vane angle and holes size directly determine the airflow distribution. While a reduced angle will weaken the recirculation zone, and a smaller size of hole will contribute a deeper jet depth. Moreover, the primary jet should be responsible to shorten the recirculation region and its location is obviously significant. Therefore, for a desired combustor, several design parameters should be appropriately adjusted, including the swirler size, vane angle, location of primary holes, and size of dilution holes, depending on the previous simulation results.

The influences of various parameters on the flow field were investigated, and a perfect model can be selected to serve as a reference in the future. The model parameters are listed in Table 5.

Table 5 Model parameters

Model	θv	Dso/mm	Lph/mm	Ddh/mm
0	50°	46	135	13
1	60°	50	135	13
2	60°	60	120	13
3	50°	60	120	13
4	60°	60	120	12
5	60°	60	120	11

θv -vane angle of swirler; Dso-outer diameter of swirler; Lph-axial distance from primary holes and injector exit; Ddh-diameter of the dilution holes

By considering the hot flow field of each model, the temperature distributions along the central axis are observed to be similar, except that of model 3, as depicted in Fig.12. The results indicate that the swirler flow increases with increasing swirler size. A decrease in vane angle can increase the flow rate; however, the swirling intensity will decrease, leading to poor recirculation. Furthermore, the location of the primary holes, also can affect the recirculation. As for the change in hole size, it was performed to adjust the airflow distribution to obtain a desired temperature field, and it can be observed that the smaller the hole size, the deeper will be the jet depth. The key indices were

calculated, and the obtained airflow distribution is summarized in Table 6. The original design was recorded as model 0, and models 1–5 denoted the remaining optimum models. Based on the previous experimental data of airflow distribution, exit temperature pattern factor, and total pressure loss, model 4 was observed to be the most optimal solution.
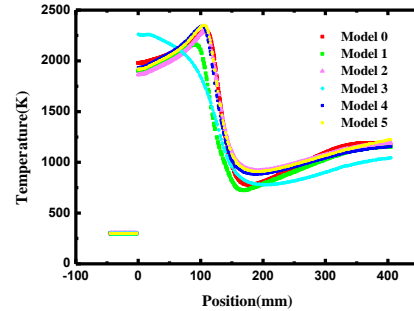

Fig. 12 Comparison of temperature along the central axis.

Table 6 Comparison between different optimizations

Model	Ws, Wph, Wdh, Wc	OTDF	ε
0	0.155,0.324,0.374,0.147	0.33	0.031
1	0.131,0.273,0.375,0.221	0.32	0.031
2	0.192,0.298,0.356,0.154	0.29	0.026
3	0.251,0.275,0.330,0.144	0.31	0.022
4	0.202,0.315,0.319,0.164	0.25	0.028
5	0.195,0.304,0.345,0.156	0.20	0.026

4.4.4 Multi-Steps Reacting Flow

The oxidation of hydrocarbons, such as methane, in air is considered to be a series of chain reactions. Therefore, chain initiation, carrying, branching, degradation, and termination must be considered when the methane combustion mechanism is analyzed and constructed. A one-step chemical mechanism can describe a complex combustion process in the easiest manner, and it demonstrates the transition between fuel molecules, which comprise a series of elementary reactions, by means of a global reaction. By contrast, it is very simple to describe the combustion process in detail. Furthermore, the detailed combustion mechanism of methane is considerably complicated, involving hundreds of elementary reactions and several intermediates, and its calculation consumes a significant amount of time and CPU resources. However, the reduced mechanism can describe the combustion process while reducing the computational time and resource requirement.

In the present study, the optimal combustor model 4 was selected for conducting the detailed simulation. A simplified mechanism (Zhao, Zhang and Yang, 2015) with 34 elementary reactions and 18 components was introduced to simulate the entire flow field and the concentration of major species, especially the radicals. The eddy-dissipation concept model was selected and solved in the

double precision format. The temperature field of the multi-steps reacting flow was depicted in Fig.13 and Fig.14.

A:
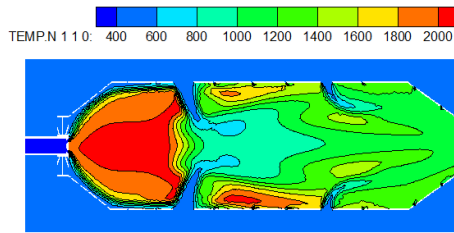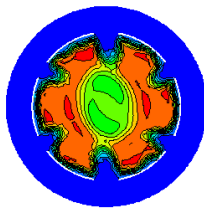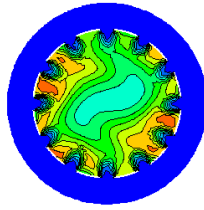
Fig. 13. Temperature field of multi-steps reacting flow (TEMP: temperature/K).
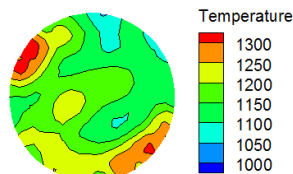

Fig. 14. Exit temperature contour.
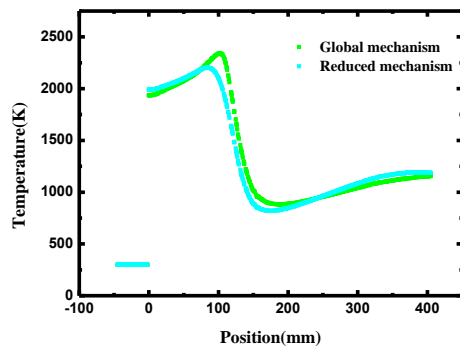
Fig. 15 Temperature along the central axis.

Comparisons were performed between the global mechanism and the reduced mechanism in the simulations conducted using model 4. The results indicated that the calculation time significantly increased with the introduction of the methane combustion mechanism. As presented in Fig.15, the temperature trend is similar to that of the global reaction. Especially, in combination with the temperature field in Fig.14, –it can be observed that the maximum temperature was approximately 2200 K, which was lower than that observed in case of

the one-step reaction by approximately 200 K. The reason was that in a single step mechanism there was no way for high-temperature formation of radicals like O, N, and OH, which consumes sensible enthalpy.

The pollutant emission rapidly increased under high temperatures in the combustion zone. Additionally, the proportion of high temperature region decreased, as depicted in Fig.14. The maximum temperature was estimated to be 1331 K, and the exit temperature pattern factor was calculated to be 0.237. These values were superior to those obtained in case of a global reaction. Thus, the result obtained using the reduced mechanism was accurate. Based on the temperature distribution of the combustion flow field, the numerical calculation of the methane combustion mechanism requires a long time; however, this is acceptable.

The mass fractions of the major species are depicted in Fig.16. According to the distribution of the OH radical in the reaction zone, the flame structure can be thoroughly determined. The hydroxide radical was observed to be mainly distributed in the central region upstream of the primary holes, and this region was triangular and slightly close to the inner surface after the primary region.
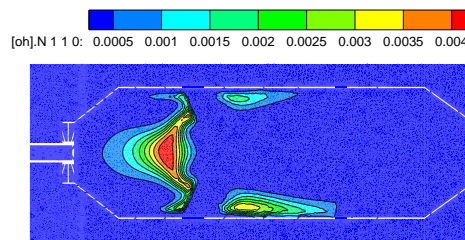

Fig.16 Mass fraction of OH.

Fig.17 indicates that a methane jet is sprayed from the conical nozzle, and it rapidly combines with the oxidant. The concentration of methane instantly decreases as the reaction proceeds. Hence, there exists an anoxic region behind the nozzle. The fuel–air ratio in the primary zone was calculated to be 0.017, which indicated a lean condition.

The mass fractions of the major products in the detailed simulation are presented in Fig.18. H_2 and H_2O are mainly concentrated in the dome region, and this region is parallel to the temperature field. In the reaction zone, insufficient oxygen content led to the generation of a large amount of CO. Furthermore, the greater the distance from the center, the higher will be the concentration of CO. The primary jet supplied plenty of fresh air to the combustion process; therefore, the unstable CO was further oxidized to CO_2. Hence, CO_2 was concentrated in the region upstream of the primary holes.
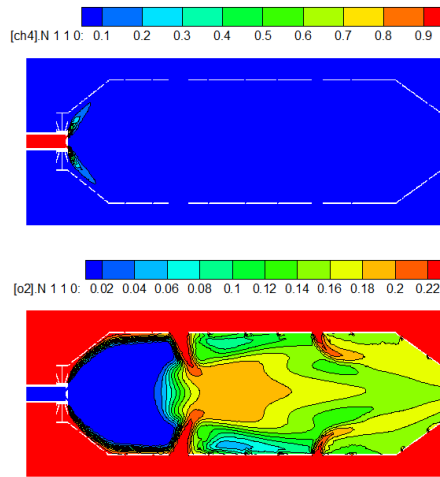
Fig. 17 Mass fraction of CH₄ and O₂.
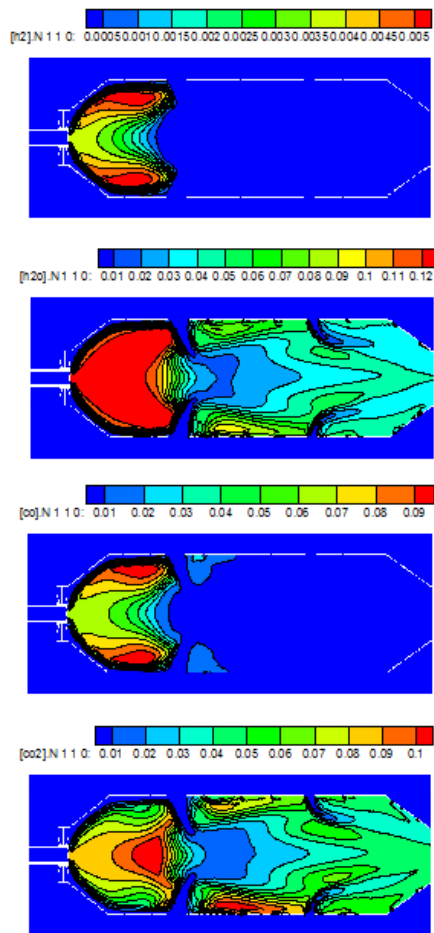
Fig. 18 Mass fractions of H₂, H₂O, CO, and CO₂.

Above all, it suggested that the distribution of the major species was reasonable. Compared with the detailed mechanism, it can be deduced that the ignition delay time of the reduced mechanism was prolonged, which warrants further investigation.

5.   CONCLUSION

In terms of the simulation of non-reacting flows, it is necessary to determine the recirculation zone in which the cold flow field is symmetrically distributed inside the combustor. The structure and location of the recirculation zone that are determined by conducting a simulation agreed well with the corresponding experimental data. Furthermore, the depths of the primary and the dilution holes were considered to be reasonable.

As for the one-step reacting flow field, a desired temperature field was formed, which confirmed the reasonability of the combustor structure. Furthermore, the cooling film protected the liner part from ablation. The additional air jets achieved their design goals as well, that is, improving the combustion efficiency and creating the desired exit temperature distribution.

According to the results of the experiment, the swirl airflow was insufficient, which led to imperfect combustion. Therefore, the combustor structure was appropriately adjusted to obtain an optimal solution.

Based on the optimization, a reduced methane combustion mechanism was introduced into subsequent simulations. The distribution of intermediates and major components as well as the accurate temperature field were observed. Although the multi-steps reaction required a longer time than that required by the global mechanism, it was more effective from the viewpoint of simulation.

Finally, the numerical data achieved a well agreement with the design data, which also verified that the experimental data can be regarded as a guide and optimization basis in the aerodynamic design process. The reasonable simulation results that are reported in this study are considerably significant from the viewpoint of guiding the design process. Additionally, further detailed and experimental investigation need to be done.

REFERENCES

Aero-engine Design Manual: Volume 11(2001). Afterburner. Aviation Industry Press.

Bulat, G. Jones, W. P. Marquis, A. and *et al.* (2011). Large Eddy Simulation of a Gas Turbine Combustion Chamber. *Mediterranean Combustion Symposium, DLR.*

Cao, P. and Li, X. J. (2018). Different shape effect of Combustion Chamber on diesel engine performance. *Automobile Applied Technology* 22, 217-219.

Ge, C., Fu, Z. G., Shi, L. and Song, J. S. (2018).Effect of swirl number on combustion and NOx formation in can-annular combustion chamber. *Journal of Engineering for Thermal Energy and Power* 12, 65-71+97.

Gordon, R. and Y. Levy (2005). Optimization of Wall Cooling in Gas Turbine Combustor through Three-Dimensional Numerical Simulation. *ASME Journal of Engineering for Gas Turbines and Power* 10, 704-723.

Habib, M. A., M. A. Nemitallah and P. Ahmed (2015).Experimental analysis of oxygen-methane combustion inside a gas turbine reactor under various operating conditions. *Energy* 86, 105-114.

He, M., Y. P. Liu and Y. W. Yan (2018). Experiment on mass flow distribution of ground gas turbine single tube combustor. *Journal of Aerospace Power* 33(04), 919-927.

Huang, Y., and Y. Z. Lin (2009). *Combustion and combustor. Beijing*, Beihang University Press.

Jiao, S. J. (1981). *Gas Turbine combustor*. Beijing: China Machine Press, 1981.

Jin, R. S. and J. Q. Suo (2016). *Advanced Gas Turbine Combustor*. Aviation Industry Press, 2016.

Jones, W. P. and B. E. Launder (1972).The prediction of laminarization with a two-equation model of turbulence. *International Journal of Heat and Mass Transfer* 15(2), 301-314.

Lefebvre, A. H. and D. R. Ballal (2010). *Gas turbine combustion*. Third Edition, CRC Press.

Li, P. F., M. Y. Xu and F. F. Wang (2017). *FLUENT GAMBIT ICEM CFD Tecplot*. Beijing, Posts & Telecom Press.

Lin, Q. H. (2013). *The development and application of the gas turbine combustors preliminary design program*. University of Chinese Academy of Sciences.

Lin, Y. Z., Q. H. Xu and G. E. Liu (2008). *Gas Turbine Combustor*. Beijing: National Defend Industry Press.

Liu, Y., P. F. Chen and J. R. Shi (2017). Effect of Installation Angle of Gas Turbine Cyclone on Outlet Temperature Quality of Combustor .*Journal of Engineering for Thermal Energy and Power* (s1), 41-45.

Magnussen, B. F. (1981). On the Structure of Turbulence and a Generalized Eddy Dissipation Concept for Chemical Reaction in Turbulent Flow. *Nineteenth AIAA Meeting*. St. Louis.

Meller, A. M. (1990). *Design of modern turbine combustor*. New York, Academic Press Inc.

Rajpara, P., A. Dekhatawala, R. Shah, and J. Banerjee (2018). Influence of fuel injection method on performance of upward swirl can-type combustor. *Applied Thermal Engineering* 130, 319-330.

Rajpara, P., A. Dekhatawala, R. Shah, and J. Banerjee (2018). Thermal and emission characteristics of reverse air flow CAN combustor. *International Journal of Thermal Sciences*.128, 175-183.

Saboohi, Z., F. Ommi, and M. Akbari (2018). Multi-objective optimization approach toward conceptual design of gas turbine combustor. *Applied Thermal Engineering* 148, 1210-1223.

Spalding, D. B. (1980).*Turbulence models*. Imperial College Report.

Xin, J. H., F. Y. Zhong (2015). Gas turbine design fundament. Profile of Shanghai Jiao Tong University Press.

Yang, W, J. Zhang (2009). Simulation of methane turbulent swirling flame in the TECFLAM combustor. *Applied Mathematical Modelling*, 33(6), 2818-2830.

Yang, M. G. (2016). *Design and Optimization of Micro Gas Turbine Combustor*. Harbin Institute of Technology.

Zhang, W. P. and Z. P. Feng (2003). Numerical Study on Combustion and Flow in a Micro Turbine Annular Combustor. *Gas Turbine Technology* 16(2), 26-30.

Zhang, W. P. and Z. P. Feng (2005). Design and study of annular combustor for micro turbine. *Proceedings of the CSEE* 25(5), 150-153.

Zhao, X. L. L. Zhang, and Z. Q. Yang (2015). Reduction and Analysis of Kinetic Model for Low Concentration Methane Homogeneous Combustion. *Journal of Engineering Thermo-physics* 36(4), 901-906.